Engineering Fracture Mechanics 271 (2022) 108594

Contents lists available at ScienceDirect

Engineering Fracture Mechanics

journal homepage: www.elsevier.com/locate/engfracmech

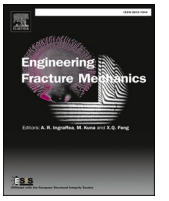

A new method for the identification of cohesive laws under pure loading modes

F. Pereira [a,*], N. Dourado [c,d], J.J.L. Morais [a], M.F.S.F. de Moura [b]

[a] CITAB/UTAD, Departamento de Engenharias, Quinta de Prados, 5001-801 Vila Real, Portugal
[b] Faculdade de Engenharia da Universidade do Porto, Departamento de Engenharia Mecânica, Rua Dr. Roberto Frias, 4200-465 Porto, Portugal
[c] CMEMS-UMinho, Departamento de Engenharia Mecânica, Universidade do Minho, Campus de Azurém, 4804-533 Guimarães, Portugal
[d] LABBELS –Associate Laboratory, Braga, Guimarães, Portugal

ARTICLE INFO

Keywords:
Composite materials
Cohesive zone model
Cohesive laws
Inverse methods

ABSTRACT

In this work, a new and simple methodology is proposed to identify the cohesive law of composite materials submitted to pure mode I and II loading. This methodology combines the experimental measured crack opening displacement and corresponding strain energy release rate with numerical simulation, using finite element method including cohesive zone modelling. The proposed procedure was tested and validated numerically, considering the determination of cohesive laws with different shapes for pure mode I and II loading. This was accomplished using the double cantilever beam (mode I) and end-notched flexure (mode II) tests. It was verified that the proposed methodology points towards the unicity of the identified solution and reproduces well the cohesive laws used as input.

1. Introduction

The accurate prediction of damage initiation and propagation in structures is becoming a research topic with increasing interest of researchers. The classical approaches are based on strength of materials methods using stress or strain failure criteria. However, these methodologies are not appropriate in the presence of discontinuities and singularities in the material, such as notches or holes, which generate important stress concentration effects. This circumstance leads to mesh dependency in numerical approaches creating significant difficulties in damage progressive analysis. In alternative, fracture mechanics based analysis can be employed. In this case, the presence of an initial material defect must be considered, which is a drawback concerning the simulation of damage onset. In order to overcome these difficulties, cohesive zone models (CZM) can be employed with success. These models combine stress-based criteria to identify damage onset and fracture mechanics concepts to deal with damage growth, thus overcoming the weaknesses and exploit the advantages of those criteria. In fact, using this strategy no initial crack is required to simulate damage initiation and the mesh dependency complications during propagation vanish. Moreover, CZM are able to handle non-linear fracture mechanics problems characterized by the presence of non-negligible fracture process zones. For these reasons, CZM are becoming popular numerical tools to deal with damage prediction in materials [2,12,14,16]. These models are based on a constitutive softening relationship between tractions and crack opening displacements, which is commonly known as the cohesive law (CL). Depending on materials fracture behavior, the CL can assume different shapes, e.g., bilinear, trilinear, trapezoidal, exponential and others. The definition of the

* Corresponding author.
E-mail addresses: famp@utad.pt (F. Pereira), nunodourado@dem.uminho.pt (N. Dourado), jmorais@utad.pt (J.J.L. Morais), mfmoura@fe.up.pt (M.F.S.F. de Moura).

https://doi.org/10.1016/j.engfracmech.2022.108594
Received 7 October 2021; Received in revised form 5 May 2022; Accepted 2 June 2022
Available online 6 June 2022

Nomenclature

Latin

a	Crack length
a_0	Initial crack length
$a_{e,i}$	Equivalent crack ($i = \mathrm{I}, \mathrm{II}$)
C_i	Compliance ($i = \mathrm{I}, \mathrm{II}$)
E_f	Elastic modulus in f direction ($f = 1, 2, 3$)
$G_{i,j}$	Strain energy release rate ($i = \mathrm{I}, \mathrm{II}$; $j = 2, 3, \ldots, n$)
G_{ic}	Critical energy release rate ($i = \mathrm{I}, \mathrm{II}$)
G_{fg}	Shear modulus in fg plane ($f, g = 1, 2, 3$) with $f < g$
h	Specimen half height
L	Half distance between supports
P_i	Load ($i = \mathrm{I}, \mathrm{II}$)
$w_{i,j}$	Crack opening displacement ($i = \mathrm{I}, \mathrm{II}$; $j = 2, 3, \ldots, n$)
k	interfacial stiffness
d	Damage parameter

Greek

$\sigma_{i,j}$	Stress ($i = \mathrm{I}, \mathrm{II}$; $j = 2, 3, \ldots, n$)
δ_i	Displacement ($i = \mathrm{I}, \mathrm{II}$)
ν_{fg}	Poisson ratio in fg plane ($f, g = 1, 2, 3$) with $f < g$
$\sigma_{u,i}$	Ultimate strength ($i = \mathrm{I}, \mathrm{II}$)

ACRONYMS

COD_i	Crack Opening Displacement ($i = \mathrm{I}, \mathrm{II}$)
DCB	Double Cantilever Beam
ENF	End-Notched Flexure
CZM	Cohesive Zone Models
CL	Cohesive Law

appropriate configuration of the CL for a given material is a fundamental aspect of the model. In the large majority of cases, the authors assume that the form of the CL is not so important [1] and adopt a pre-established shape. However, this procedure is not rigorous and can become rather inaccurate, mainly in cases where material fracture behavior is totally unknown a priori. In order to solve this difficulty, the determination of the CL shape should be performed. In general, two main procedures are employed with this aim: the inverse and direct methods. The inverse methods lay on assuming a pre-established law shape and the identification of the corresponding cohesive parameters is accomplished employing fitting procedures that use a manual iterative procedure [5], or involve automatic optimization strategies ([8;13]. Through the later, the most used process employs an optimization technique aiming to fit the numerical load-displacement curve with the experimental one, through minimization of an objective function quantifying the difference between those curves [4;8;15,17]. A more complex approach requires the displacement field at the crack tip, measured by high-performance optical instruments, which is used as input in the numerical model aiming to simulate the global behavior [11,13]. In both cases, several problems can be pointed. In effect, too many iterations are usually necessary until a good reproducibility of the experimental curve is achieved. In addition, the usual unevenness observed in the experimental curves can induce difficulties in the automatic optimization process. Finally, it is frequently pointed the lack of unicity of the found solution [3,10] that increases with the complexity of the CL shape (i.e., the number of the parameters to be identified).

The direct method lies on experimental determination of the CL [7], which involves the monitoring of the crack tip opening displacements (COD) during the test. The CL is obtained by differentiation of the relation between strain energy release rate and COD, which requires the fitting of an appropriate function. This method has two main advantages relative to inverse procedures: (i) it does not require the pre-definition of CL shape; (ii) the resulting law is obtained based on local measurements, which are better representative of the fracture phenomenon. However, it has been observed that resulting CL is sensitive to the function adjusted to the strain energy release rate versus COD relation [20].

The objective of this work is to propose a new and simple methodology to determine the CL. The method combines experimental data with numerical simulation using finite element analysis including cohesive zone modelling. The proposed procedure was validated numerically considering the determination of the CL under pure mode I loading using the double cantilever beam (DCB) test and under pure mode II loading employing the end-notched flexure (ENF) test. In both cases, several CLs were considered as input and the suitability of the model to reproduce them was verified.

2. Cohesive zone model

The cohesive zone model used in this work is based on piecewise linear softening CL (Fig. 1). A stepwise softening law with several branches can be used to replicate with accuracy the fracture behaviour of most materials. Hence, before damage onset, the relation between normal or shear traction (σ_i) and corresponding relative displacement (w_i) writes

$$\sigma_i = k w_i \;\; ; \;\; (i = \mathrm{I},\, \mathrm{II}) \tag{1}$$

where k is the interfacial stiffness. This parameter usually assumes a high value (10^6-10^7 N/mm^3) to avoid unwanted interpenetrations during contact. Therefore, the relative displacement corresponding to damage onset ($w_{i,1}$) becomes quite small and it was neglected in the schematic representation of Fig. 1. After damage onset, the softening relationship is described by

$$\sigma_i = (1\text{-}d) k w_i \;\; ; \;\; (i = \mathrm{I},\, \mathrm{II}) \tag{2}$$

being d the damage parameter, ranging between zero and one. The crack opening displacements and tractions at the transition points ($j = 2,\, 3,\, \ldots n$) (Fig. 1) are employed to define the cohesive law.

Equating the critical energy release rate (G_{ic}) to the area of the softening law (Fig. 1) it is possible to determine the ultimate relative displacement for $j = n$ in the following equation, provided that the coordinates of the several inflection points ($w_{i,j}$, $\sigma_{i,j}$) are previously determined following the methodology described in the next section,

$$G_{ic} = \sum_{j=2}^{n} \frac{(\sigma_{i,j} + \sigma_{i,(j-1)})(w_{i,j} - w_{i,(j-1)})}{2} \tag{3}$$

The expression of the damage parameter on the several segments can now be easily obtained equating the corresponding softening relation,

$$\sigma_i = \frac{\sigma_{i,j} - \sigma_{i,(j-1)}}{w_{i,j} - w_{i,(j-1)}} \left(w_i - w_{i,(j-1)}\right) + \sigma_{i,(j-1)} \quad \text{for} \quad w_{i,(j-1)} \le w_i \le w_{i,j} \tag{4}$$

to Eq. (2), and solving each equation in order to parameter d. This leads to the following relationship,

$$d = 1 - \frac{1}{k w_i} \left[\frac{\sigma_{i,j}\left(w_i - w_{i,(j-1)}\right) + \sigma_{i,(j-1)}\left(w_{i,j} - w_i\right)}{w_{i,j} - w_{i,(j-1)}} \right] \quad \text{for} \quad w_{i,(j-1)} \le w_i \le w_{i,j} \tag{5}$$

Giving this relation, damage progression is simulated differently according to the successive stages (branches) of damage evolution.

3. Identification of the cohesive law

The proposed methodology is based on the ultimate strength ($\sigma_{i,1}$) and on the relation between the strain energy release rate (G_i), and crack opening displacements (COD_i). The first step consists in the determination of traction values in the vertices of the softening region ($\sigma_{i,j}$ in Fig. 1), as a function of the ultimate strength according to the following equations,

$$\sigma_{i,j} = \frac{2\left(G_{i,j} - G_{i,(j-1)}\right)}{w_{i,j} - w_{i,(j-1)}} - \sigma_{i,1} \quad \text{for} \quad j = 2$$

$$\sigma_{i,j} = \frac{2\left(G_{i,j} - G_{i,(j-1)}\right)}{w_{i,j} - w_{i,(j-1)}} + (-1)^{j-1}\sigma_{i,1} - (-1)^{j-1} \sum_{k=1}^{j-2} (-1)^{k-1} \frac{2\left(G_{i,(k+1)} - G_{i,k}\right)}{w_{i,(k+1)} - w_{i,k}} \quad \text{for} \quad j > 2 \tag{6}$$

Using this information and imposing the following constraints,

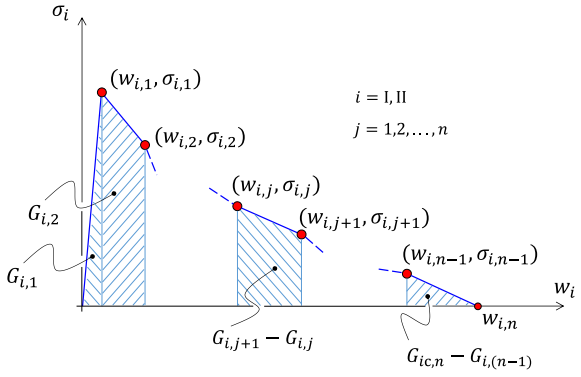

Fig. 1. Piecewise linear cohesive law ($G_{ic} = \sum_{j=2}^{n} G_{i,j}$).

$$\sigma_{i,j} > 0, \quad j = 1, 2, 3, \cdots, n$$

$$\sigma_{i,j} > \sigma_{i,(j+1)}, \quad j = 1, 2, 3, \cdots, n \tag{7}$$

the allowable domain for the ultimate strength ($\sigma_{1,i}$) is therefore identified, making the seeking strategy a single variable problem. Fig. 2 shows a schematic representation of the proposed methodology to identify the ultimate strength ($\sigma_{i,1}$) search domain bearing in mind a softening law with five vertices, i.e., a total of four branches. Considering Eqs. (6), it is possible to plot the linear relations between the intermediate components of tractions ($\sigma_{i,j}$ with $j = 2, 3, 4$) in function of $\sigma_{i,1}$(Fig. 2). Subsequently, the constraints given by Eqs. (7) are imposed, aiming to define the allowable domain for this cohesive parameter ($\sigma_{i,1}$) (dashed region in Fig. 2).

It should be noted that the increase of the number of branches, with consequent reduction of tractions range between the selected vertices, leads to a reduction of the allowable domain of the ultimate strength. The determination of this value ($\sigma_{i,1}$) in the allowable and limited region (dashed area in Fig. 2) is accomplished by minimization of the difference between the numerical and experimental load-displacement curves. This procedure is much less sensitive to lack of uniqueness problems in comparison with the classic inverse method relying on the fitting of numerical to experimental load-displacement curves. In fact, the proposed procedure constitutes a single variable seeking technique and an accurate solution can be found after some iterations. Fig. 3 presents a flowchart of the implemented algorithm revealing the main steps and their sequence of the proposed procedure.

For the application of the described procedure it is important to determine the evolution of G_i during the mechanical test. The strain energy release rate can be obtained by means of an equivalent crack length procedure. In the DCB case ([8]), the specimen compliance versus crack length relation can be obtained from the Timoshenko beam theory,

$$C_{\mathrm{I}} = \frac{8a^3}{E_1 B h^3} + \frac{12a}{5BhG_{13}} \tag{8}$$

where B, h, a stand for specimen dimensions (Fig. 4a and 5a) and E_1 and G_{13} are the material elastic properties (Table 1). An equivalent crack length is obtained as a function of the current compliance, $a_{\mathrm{e}} = \mathrm{f}(C_{\mathrm{I}})$. The solution can be found by the following equation,

$$\alpha a_{\mathrm{e}}^3 + \beta a_{\mathrm{e}} + \gamma = 0 \tag{9}$$

where α and β are the coefficients multiplying a_{e}^3 and a_{e}, respectively and $\gamma = -C_{\mathrm{I}}$. Using the Matlab® software and only keeping the real solution yields,

$$a_{\mathrm{e}} = \frac{1}{6\alpha} A - \frac{2\beta}{A} \tag{10}$$

with α, β and A defined as,

$$\alpha = \frac{8}{Bh^3 E}; \beta = \frac{12}{5BhG}; A = \left((-108\gamma + 12\sqrt{3\left(\frac{4\beta^3 + 27\gamma^2\alpha}{\alpha}\right)})\alpha^2\right)^{\frac{1}{3}} \tag{11}$$

This equivalent crack length is longer than the actual one since it accounts for root rotation effects and the development of the fracture process zone ahead of the crack tip. Combining Eq. (8) with the Irwin-Kies relation,

$$G_{\mathrm{I}} = \frac{P^2}{2B}\frac{dC}{da} \tag{12}$$

it leads to

$$G_{\mathrm{I}} = \frac{6P^2}{B^2 h}\left(\frac{2a_e^2}{h^2 E_1} + \frac{1}{5G_{13}}\right) \tag{13}$$

This procedure provides the evolution of G_{I} in the course of the test, using only data ensuing from the load-displacement curve. In the case of the ENF test [6], the specimen compliance writes,

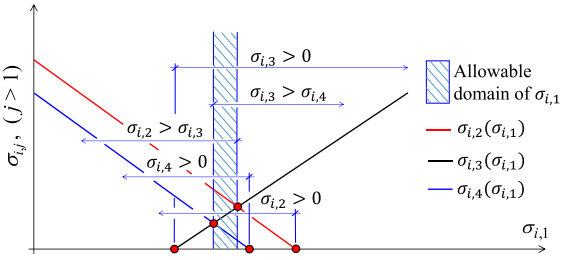

Fig. 2. Schematic representation of the resulting domain for $\sigma_{1,\mathrm{i}}$ assuming four vertices ($j = 5$ in Fig. 1).

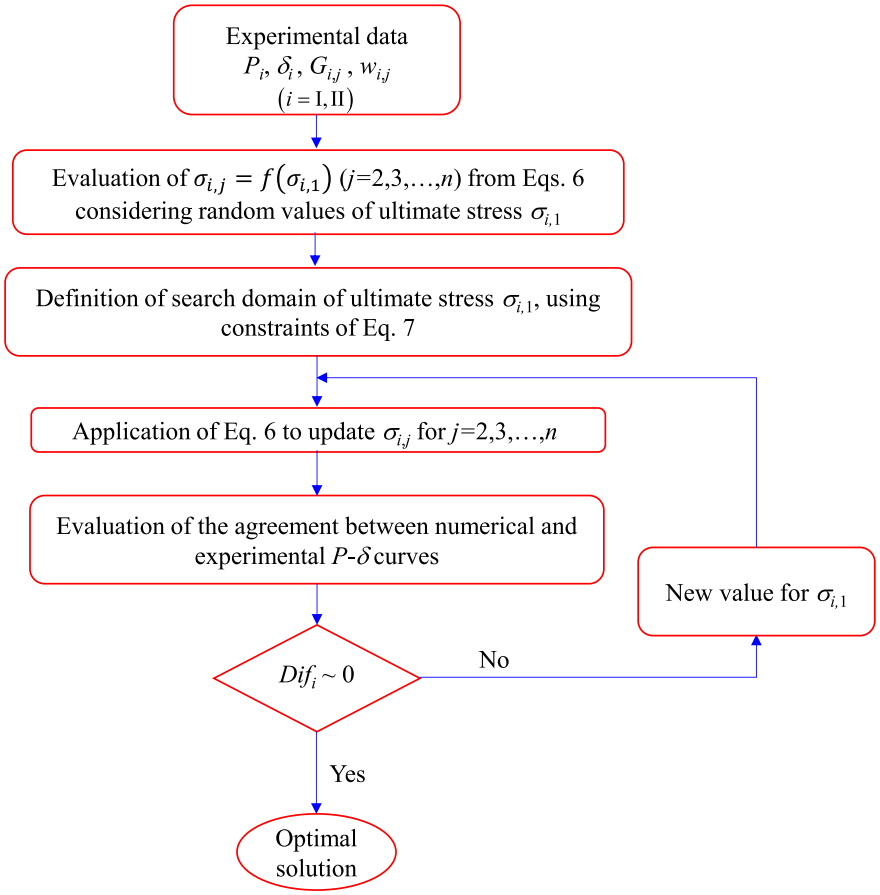

Fig. 3. Flowchart of the developed algorithm used to obtain the cohesive law.

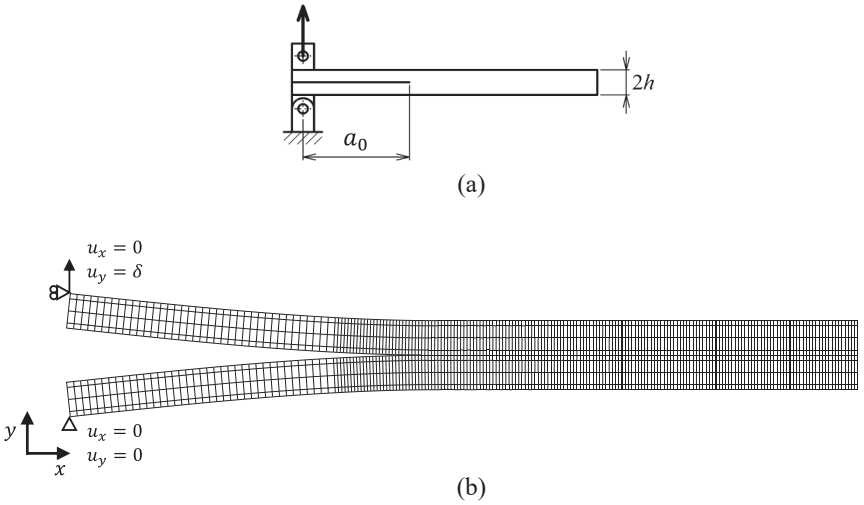

Fig. 4. (a) Schematic representation of the DCB test (dimensions in mm: $a_0 = 45; h = 2.7,$ width $B = 15$) and (b) used finite element mesh.

Table 1
Typical elastic properties of carbon-epoxy [8].

$E_1 = 109$ GPa	$\nu_{12} = 0.34$	$G_{12} = 4315$ MPa
$E_2 = 8819$ MPa	$\nu_{13} = 0.34$	$G_{13} = 4315$ MPa
$E_3 = 8819$ MPa	$\nu_{23} = 0.38$	$G_{23} = 3200$ MPa

$$C_{II} = \frac{3a^3 + 2L^3}{8E_1Bh^3} + \frac{3L}{10G_{13}Bh} \tag{14}$$

which allows to determine the equivalent crack length

$$a_e = \left[\left(C_{II} - \frac{3L}{10G_{13}Bh}\right)\frac{8E_1Bh^3}{3} - \frac{2L^3}{3}\right]^{1/3} \tag{15}$$

Combining Eqs. (15) and (12), the mode II strain energy release rate becomes,

$$G_{II} = \frac{9P^2a_e^2}{16E_1B^2h^3} \tag{16}$$

4. Numerical model

Finite element analyses of the double cantilever beam (DCB) and end-notched flexure (ENF) tests were performed (Figs. 4 and 5). A two-dimensional analysis considering 1800 solid plane strain 8-node elements were used to simulate carbon-epoxy material (Tables 1 and 2), connected by means of compatible 200 cohesive elements with 6 nodes located at the specimen mid-height, aiming to simulate damage initiation and propagation. Non-linear geometrical analyses considering very small increments (0.0005 mm) for the loading applied displacement were assumed to simulate a quasi-static loading. The applied displacement was assumed equal to 10 mm to guarantee self-similar crack growth in all cases analysed.

5. Results and discussion

Different cohesive laws were used as input in the numerical analyses to perform the virtual tests. The crack opening displacement (COD_i, i = I, II) is measured in the numerical analysis at the pair of homologous points (above and below the crack line) located at the crack tip. Experimentally, they can be monitored by means of the digital image correlation [20]. These parameters allow to stablish the relations $G_i = f(COD_i)$ (Fig. 6), which are essential for the above described procedure.

A comparison between the cohesive law identification method developed by [18], in the following designated as "old algorithm", and the method proposed in this work, named as "new algorithm", was made. The "old algorithm" consists of an inverse method based on the combination of numerical simulations with an optimization algorithm aiming to minimize the difference between numerical and experimental load-displacement curves in each iteration. With this purpose, the pairs traction value ($\sigma_{i,j}$) and relative displacement ($w_{i,j}$) that define a cohesive law composed by four linear branches are iteratively changed envisaging the best agreement between the numerical and experimental load-displacement curves.

The two algorithms were applied to a DCB test considering a polynomial softening law and both provide a good agreement on load-displacement curves (Fig. 7a). Anyway, a detailed analysis of the load-displacement curves close to peak loads reveals that the new algorithm, considering $j = 5$ (Figs. 1 and 2), provides a better reproduction of the reference curve (Fig. 7b). Regarding the cohesive

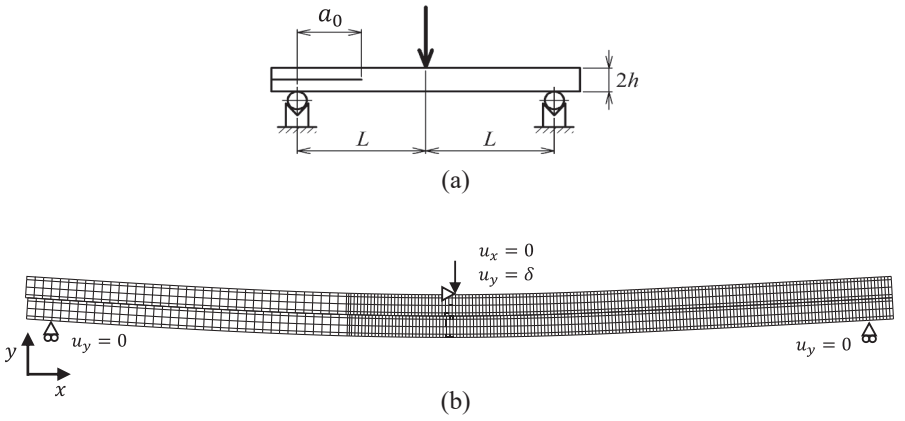

Fig. 5. (a) Schematic representation of the ENF test (dimensions in mm: $a_0 = 75$; $h = 2.7$, width $B = 15$; $L = 100$) and (b) used finite element mesh.

Table 2
Cohesive parameters of carbon-epoxy [6].

Mode I	Mode II
$\sigma_{uI} = 50$ MPa $G_{Ic} = 0.3$ N/mm	$\sigma_{uII} = 50$ MPa $G_{IIc} = 0.7$ N/mm

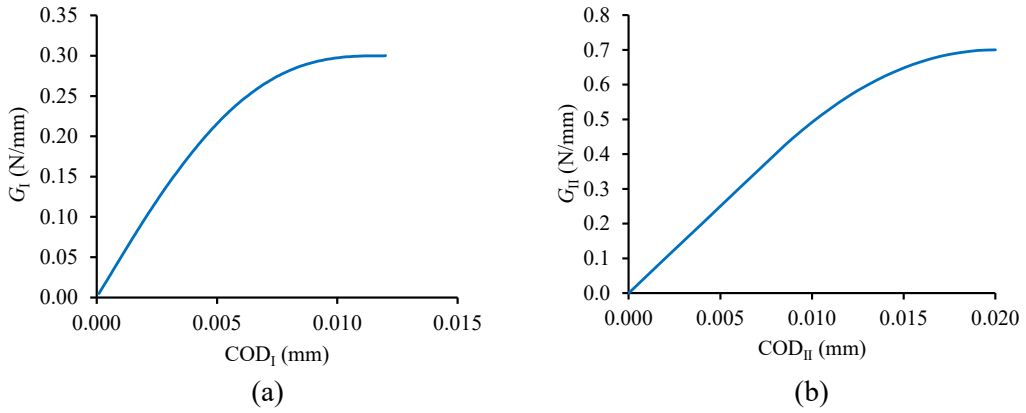

Fig. 6. Strain energy release rate as a function of the crack opening displacement: (a) Mode I ($G_I = f(COD_I)$); (b) Mode II ($G_{II} = f(COD_{II})$).

laws, the old algorithm identified a softening law considerably different of the reference one. This highlights the difficulty of ensuring a unique solution from an adjustment based only on load-displacement curve. Another important issue is the CPU time consuming to achieve a solution. Both algorithms can be considered fast, however the new algorithm provides a solution in less than five iterations, which represents a decrease around 50% (Fig. 8).

Four common cohesive laws (CLs) representative of fracture behaviour of different composite materials were analysed to verify the model performance: the linear, the bilinear, the trapezoidal and the polynomial. Applying the data reduction methods described by the end of section 3. The respective *Resistance*-curves (*R*-curves) are presented in Fig. 9. As expected the values given by the plateau regions are in close agreement reflecting self-similar crack propagation under constant fracture energies (G_{Ic} and G_{IIc} for mode I and mode II, respectively).

The piecewise linear softening law with four branches described in section 2 was employed to reproduce the considered CLs, in Figs. 10 and 11 it is possible to visualize the pairs (w,σ) used as input. In the mode I case, the bilinear and polynomial CLs were selected and the other ones (i.e., the linear and trapezoidal) were considered for mode II loading. Figs. 10 and 11 illustrate the agreement obtained for the referred four CLs. In the mode I case, both methods were considered, and it can be verified that the new algorithm captures well the reference law used as input. Instead, the old algorithm propitiates remarkable different softening laws when compared with the input ones.

In order to verify whether the excellent performance of the new algorithm obtained for mode I keeps valid for the mode II loading case, the procedure was applied to the linear and trapezoidal softening laws frequently used for this shear loading mode [9,19]. The results obtained are plotted in Fig. 11 confirming the excellent performance of the proposed methodology on the evaluation of the cohesive laws under pure loading modes.

6. Conclusions

In this work, a new and simple methodology allowing the determination of cohesive laws representative of the fracture behaviour of composite materials under pure mode I and II loading was developed. The procedure involves experimental data in combination with finite element analysis including cohesive zone modelling. The method requires the monitoring of the load-displacement and the crack opening displacement (COD_i, i = I, II) during the fracture test. From the load-displacement data, the strain energy release rate (G_i) in the course of the pure mode fracture tests (DCB and ENF) is obtained employing an equivalent crack length data reduction scheme, which allows to establish the $G_i = f(COD_i)$ relation. Subsequently, a piecewise linear cohesive law is used in a finite element analysis imposing several conditions that restrict the possible domain for the local strength. An optimization algorithm that minimizes the difference between the numerical and experimental load-displacement curves performs the final identification of this parameter. This inverse procedure englobes a single variable seeking, which means that it shows low sensitivity to lack of unicity of the found solution.

The method was tested considering four typical different cohesive laws, being two applied to pure mode I loading and the other two to the pure mode II loading, performing virtual DCB and ENF tests (mimicking experimental data), respectively. The ensuing $G_i = f(COD_i)$ relations and the respective load-displacement curves were used in the seeking procedure. A piecewise linear softening law

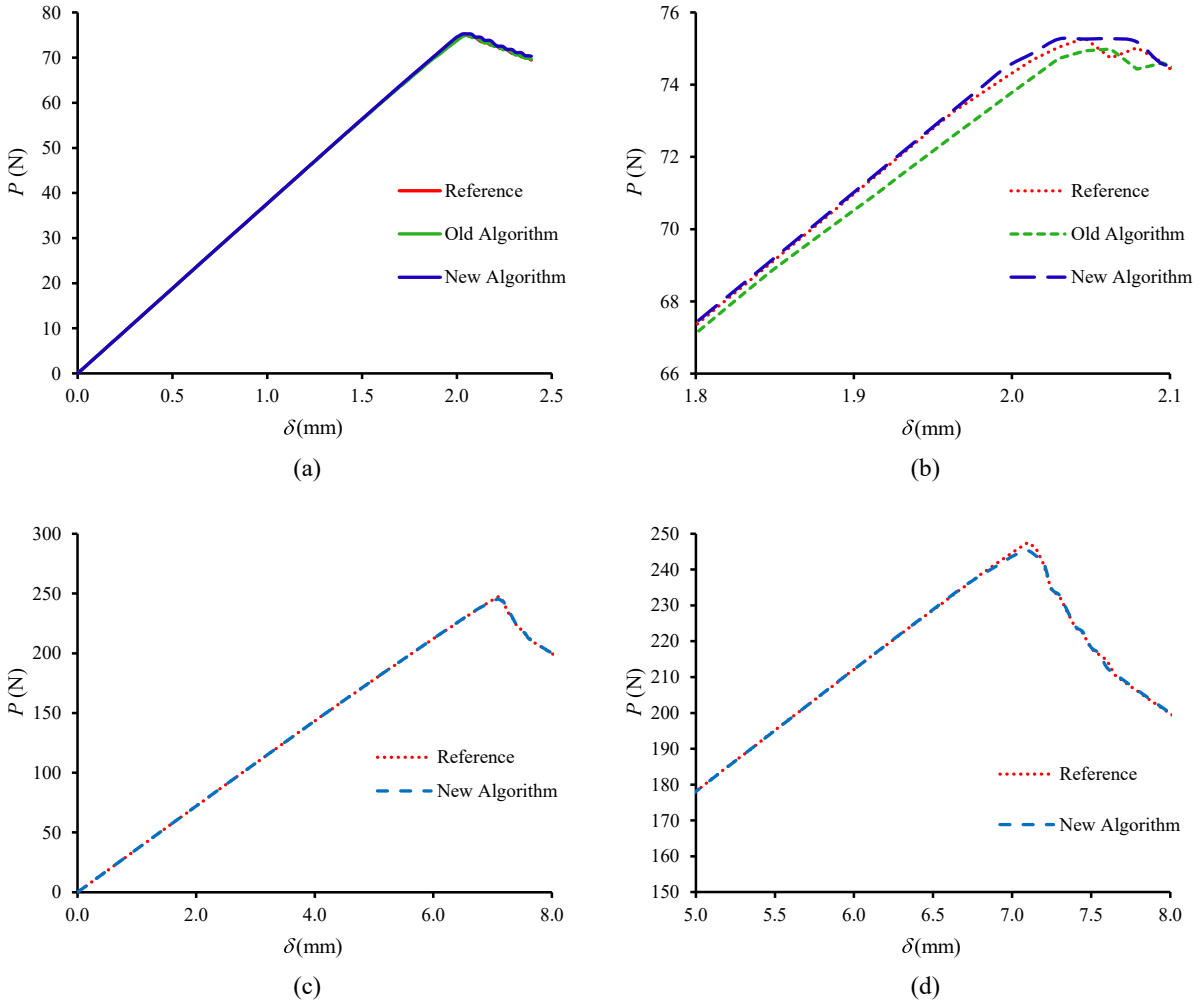

Fig. 7. a) Mode I load-displacement curve (polynomial cohesive law) b) detail close to peak loads; c) Mode II load-displacement curve (linear cohesive law) d) detail close to peak loads.

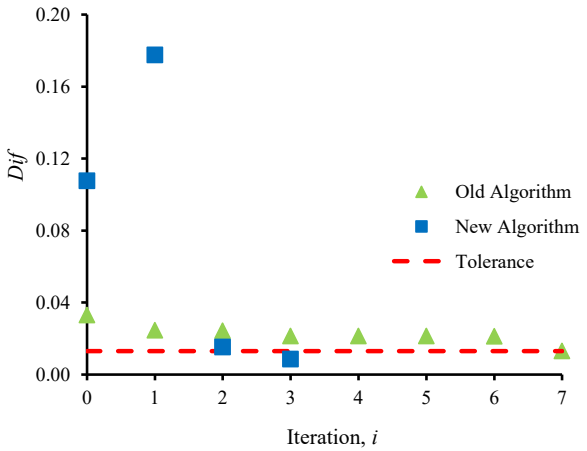

Fig. 8. Convergence analysis during iteration process.

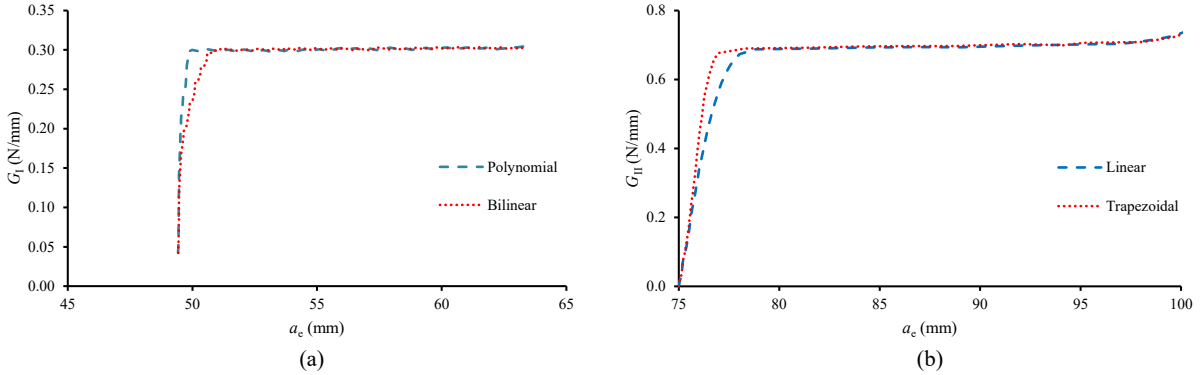

Fig. 9. a) Mode I and b) mode II *R*-curves ensuing from the employed cohesive laws.

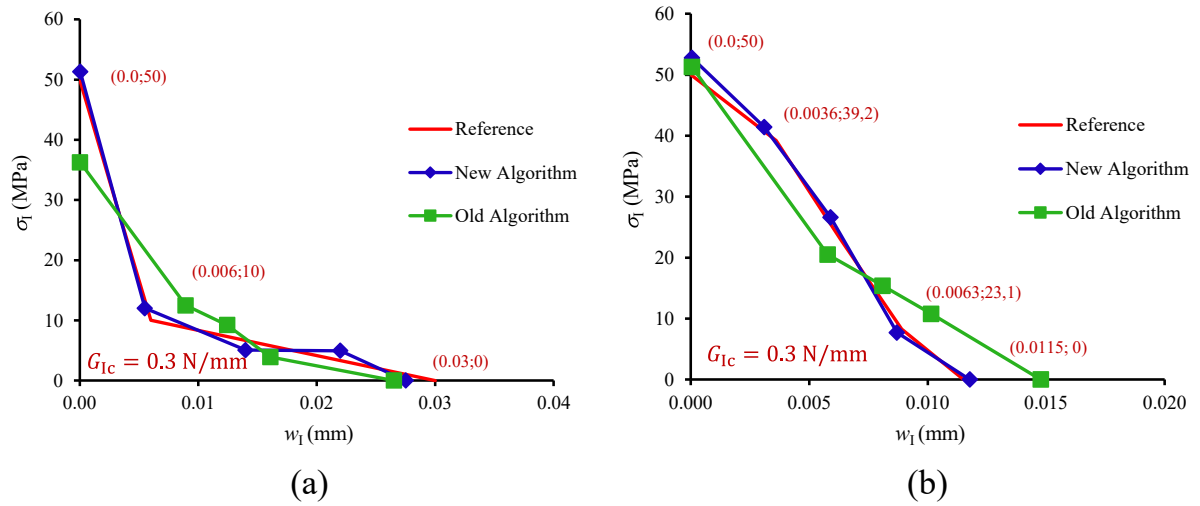

Fig. 10. Bilinear (a) and polynomial (b) CLs used for mode I loading.

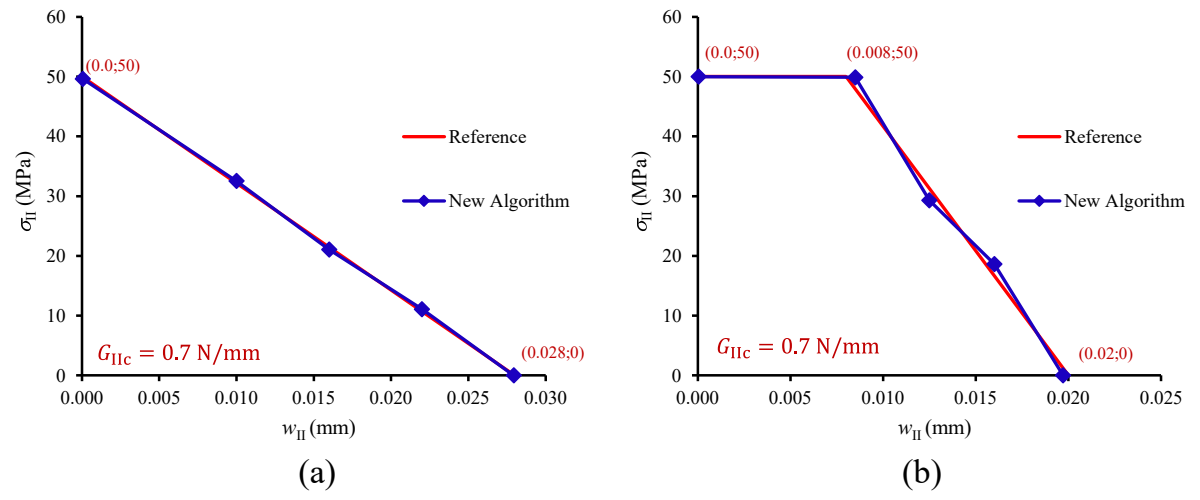

Fig. 11. Linear (a) and trapezoidal (b) CLs used for mode II loading.

with four branches was used to capture the CLs used in the virtual test simulations. Overall, excellent agreement was obtained between the cohesive laws used as input and the ensuing ones resulting from the employed procedure, which makes the presented procedure a valuable tool regarding the identification of the cohesive laws representative of materials' fracture. In fact, the proposed methodology can be easily implemented for coherent cohesive law assessment of any material with reduced computational costs owing to the set of the imposed restrictions.

CRediT authorship contribution statement

F. Pereira: Methodology, Conceptualization, Investigation, Writing-Original draft, Software, Data Curation, Funding acquisition. **N. Dourado:** Formal analysis, Data Curation, Review & Editing, Funding acquisition. **J.J.L. Morais:** Methodology, Conceptualization, Investigation, Funding acquisition. **M.F.S.F. de Moura:** Methodology, Investigation, Software, Funding acquisition.

Declaration of Competing Interest

The authors declare that they have no known competing financial interests or personal relationships that could have appeared to influence the work reported in this paper.

Acknowledgments

The first and third author acknowledges the Portuguese Foundation for Science and Technology, under the project UIDB/04033/2020. The second author acknowledges FCT for the conceded financial support through the reference projects PTDC/EME-SIS/28225/2017 and UID/EEA/04436/2019. The fourth author acknowledges the "Laboratório Associado de Energia, Transportes e Aeronáutica" (LAETA) for the financial support by the project UID/EMS/50022/2013, and to the funding of Project NORTE-01-0145-FEDER-000022 - SciTech - Science and Technology for Competitive and Sustainable Industries, co-financed by Programa Operacional Regional do Norte (NORTE2020), through Fundo Europeu de Desenvolvimento Regional (FEDER).

References

[1] Alfano G. On the influence of the shape of the interface law on the application of cohesive-zone models. Compos. Sci. Technol. Adv Statics Dynamics Delamination 2006;66:723–30. https://doi.org/10.1016/j.compscitech.2004.12.024.
[2] Balzani C, Wagner W. An interface element for the simulation of delamination in unidirectional fiber-reinforced composite laminates. Eng Fract Mech Fract Compos Mater 2008;75:2597–615. https://doi.org/10.1016/j.engfracmech.2007.03.013.
[3] Cordeiro SGF, Leonel ED, Beaurepaire P. Quantification of cohesive fracture parameters based on the coupling of Bayesian updating and the boundary element method. Eng Anal Bound Elem 2017;74:49–60. https://doi.org/10.1016/j.enganabound.2016.10.010.
[4] Cox BN, Yang Q. Cohesive zone models of localization and fracture in bone. Eng Fract Mech Fract Mater: Moving Forwards 2007;74:1079–92. https://doi.org/10.1016/j.engfracmech.2006.12.024.
[5] de Moura MFSF, Campilho RDSG, Gonçalves JPM. Crack equivalent concept applied to the fracture characterization of bonded joints under pure mode I loading. Compos Sci Technol 2008;68:2224–30. https://doi.org/10.1016/j.compscitech.2008.04.003.
[6] de Moura MFSF, de Morais AB. Equivalent crack based analyses of ENF and ELS tests. Eng. Fract. Mech. Fract Compos Mater 2008;75:2584–96. https://doi.org/10.1016/j.engfracmech.2007.03.005.
[7] de Moura MFSF, Gonçalves JPM, Magalhães AG. A straightforward method to obtain the cohesive laws of bonded joints under mode I loading. Int J Adhes Adhes 2012;39:54–9. https://doi.org/10.1016/j.ijadhadh.2012.07.008.
[8] de Moura MFSF, Morais JJL, Dourado N. A new data reduction scheme for mode I wood fracture characterization using the double cantilever beam test. Engng Fract Mech 2008;75:3852–65. https://doi.org/10.1016/j.engfracmech.2008.02.006.
[9] Dourado N, de Moura MFSF, de Morais AB, Pereira AB. Bilinear approximations to the mode II delamination cohesive law using an inverse method. Mech Mater 2012;49:42–50. https://doi.org/10.1016/j.mechmat.2012.02.004.
[10] Ferreira MDC, Venturini WS. Inverse analysis FOR two-dimensional structures using the boundary element method. Adv Engng Softw 2010;41:1061–72. https://doi.org/10.1016/j.advengsoft.2010.04.003.
[11] Ferreira MDC, Venturini WS, Hild F. On the analysis of notched concrete beams: From measurement with digital image correlation to identification with boundary element method of a cohesive model. Engng Fract Mech 2011;78:71–84. https://doi.org/10.1016/j.engfracmech.2010.10.008.
[12] Harper PW, Sun L, Hallett SR. A study on the influence of cohesive zone interface element strength parameters on mixed mode behaviour. Compos Part Appl Sci Manuf 2012;43:722–34. https://doi.org/10.1016/j.compositesa.2011.12.016.
[13] Hong S, Kim K-S. Extraction of cohesive-zone laws from elastic far-fields of a cohesive crack tip: a field projection method. J Mech Phys Solids 2003;51:1267–86. https://doi.org/10.1016/S0022-5096(03)00023-1.
[14] Kumar D, Roy R, Kweon J-H, Choi J. Numerical Modeling of Combined Matrix Cracking and Delamination in Composite Laminates Using Cohesive Elements. Appl Compos Mater 2016;23:397–419. https://doi.org/10.1007/s10443-015-9465-0.
[15] Maier G, Bocciarelli M, Fedele R. Some innovative industrial prospects centered on inverse analyses. In: Mróz Z, Stavroulakis GE, editors. CISM International Centre for Mechanical SciencesParameter Identification of Materials and Structures. Vienna: Springer; 2005. p. 55–93.
[16] Mohammadi B, Salimi-Majd D. Investigation of delamination and damage due to free edge effects in composite laminates using cohesive interface elements. Eng Solid Mech 2014;2(2):101–18.
[17] Oh J-C, Kim H-G. Inverse estimation of cohesive zone laws from experimentally measured displacements for the quasi-static mode I fracture of PMMA. Engng Fract Mech 2013;99:118–31. https://doi.org/10.1016/j.engfracmech.2012.11.002.
[18] Pereira FAM, de Moura MFSF, Dourado N, Morais JJL, Xavier J, Dias MIR. Direct and inverse methods applied to the determination of mode I cohesive law of bovine cortical bone using the DCB test. Int J Solids Struct 2017;128:210–20. https://doi.org/10.1016/j.ijsolstr.2017.08.028.
[19] Reis JP, de Moura MFSF, Moreira RDF, Silva FGA. Pure mode I and II interlaminar fracture characterization of carbon-fibre reinforced polyamide composite. Compos Part B Eng. 2019;169:126–32. https://doi.org/10.1016/j.compositesb.2019.03.069.
[20] Xavier J, Oliveira M, Monteiro P, Morais JJL, de Moura MFSF. Direct Evaluation of Cohesive Law in Mode I of Pinus pinaster by Digital Image Correlation. Exp Mech 2014;54:829–40. https://doi.org/10.1007/s11340-013-9838-y.